JOURNAL OF GEOPHYSICAL RESEARCH, VOL. 93, NO. B11, PAGES 13,251-13,264, NOVEMBER 10, 1988

ABSENCE OF EVIDENCE FOR A SHALLOW MAGMA CHAMBER BENEATH LONG VALLEY CALDERA, CALIFORNIA, IN DOWNHOLE AND SURFACE SEISMOGRAMS

Egill Hauksson

Department of Geological Sciences, University of Southern California, Los Angeles

Abstract. A downhole seismometer at 900-m depth and a temporary network of surface stations were deployed to use rays from local microearthquakes to study the upper and middle crust beneath the Long Valley caldera. The downhole seismograms show S waves with high apparent amplitudes from earthquakes located 2-20 km to the south of the downhole seismometer. In contrast, S waves from earthquakes located in the distance range 20-30 km to the south have low apparent amplitudes. If P and S amplitudes are normalized relative to the respective coda amplitudes, the S to coda amplitude ratios appear to remain constant but the P to coda amplitude ratios vary significantly with takeoff angle. A comparison of the calculated radiation patterns for a double couple in a uniform halfspace and focal mechanisms of the recorded earthquakes suggest that the observed variations in P and S amplitudes are caused by radiation pattern effects. Reanalysis of possible travel time delays found by Elbring and Rundle (1986), who used a subset of the borehole data analyzed in this study, shows that they underestimated the epicentral distances to three of the earthquakes and hence generated an artificial kink in the reduced travel time versus depth curve. Synthetic calculations of reduced travel time versus depth suggest that an apparent velocity of 5.7 km/s gives less scatter than 6.0 km/s used by Elbring and Rundle (1986). Plots of ts/tp versus depth show that contrary to the findings of Elbring and Rundle (1986), the Vp/Vs ratio stays fairly constant with depth and a small (<3-km diameter) magma chamber cannot easily be resolved. Furthermore, combined analysis of downhole and surface data shows that neither data set requires a low-velocity zone or a zone of anomalously high Vp/Vs at depth below the Casa Diablo area.

Introduction

From September 19 to October 10, 1984, 14 digital recorders were deployed, each with a three-component seismometer, to record local earthquakes in Long Valley, California. The instruments were deployed in two separate clusters. The first cluster of nine instruments was located in the Casa Diablo region above a postulated magma chamber [Sanders, 1984]. The second cluster of instruments located 7 km to the north of Casa Diablo and just south of Lookout Mountain, included a three-component seismometer deployed in a 900-m-deep borehole OLV-1. (Figure 1). During the recording period, 32 local earthquakes were detected by both the USGS seismic network in Long Valley and by the downhole as well as several surface instruments in the Casa Diablo area.

The downhole seismometer and the tightly clustered surface network of seismometers were deployed to use rays from local microearthquakes to study the upper and middle crust (0-15 km depth) beneath the southern half of Long Valley caldera (Figure 1). Because the rays from microearthquakes originate at depth, they are better sources of energy for transmission through, or reflection off, a magma body at shallow crustal depths than rays generated at the surface in conventional refraction or reflection surveys. Also, microearthquakes, which can be modeled as point sources, are efficient generators of S waves. Case studies, such as (1) Rio Grande Rift near Socorro, New Mexico [Rinehart et al., 1979], (2) Mount Katmai, Alaska [Matumoto, 1971]; (3) Krafla volcano in Iceland [Einarsson, 1978], and (4) Long Valley, California [Ryall and Ryall, 1981; Sanders and Ryall, 1983; Sanders, 1984], have used secondary reflected phases or anomalous attenuation of S waves from microearthquakes to infer the presence of subsurface magma chambers. When using this method, however, both a sufficient spatial distribution of microearthquakes and a dense seismic network are needed to determine the detailed structure of the magma chamber.

Steeples and Iyer [1976] used delays of teleseimic P waves to show that a zone of lower velocity, 5-15% lower than the velocity of the region surrounding the caldera, probably existed between 7-and 25-km depth below Long Valley caldera. They, however, could not resolve the exact location or detailed shape of possible magma chambers. Since then, postulated magma chambers beneath the Long Valley caldera have been mapped using qualitative techniques by Ryall and Ryall [1981], Sanders and Ryall [1983], and Sanders [1984]. These studies assumed straight-line ray paths between the epicenters and the respective station, and classified the ray paths according to the amplitude and frequency content of recorded P and S waves. The proposed magma chamber that is best constrained from their studies is located below the Casa Diablo area. Independent evidence for possible subsurface magma bodies has also been observed in some seismic refraction lines [e.g., Hill, 1976; Hill et al., 1985]. In addition, geodetic data and gravity data from the Long Valley caldera have been modeled in terms of inflating magma chambers at

Paper number 7B2045.
0148-0227/88/007B-2045$05.00

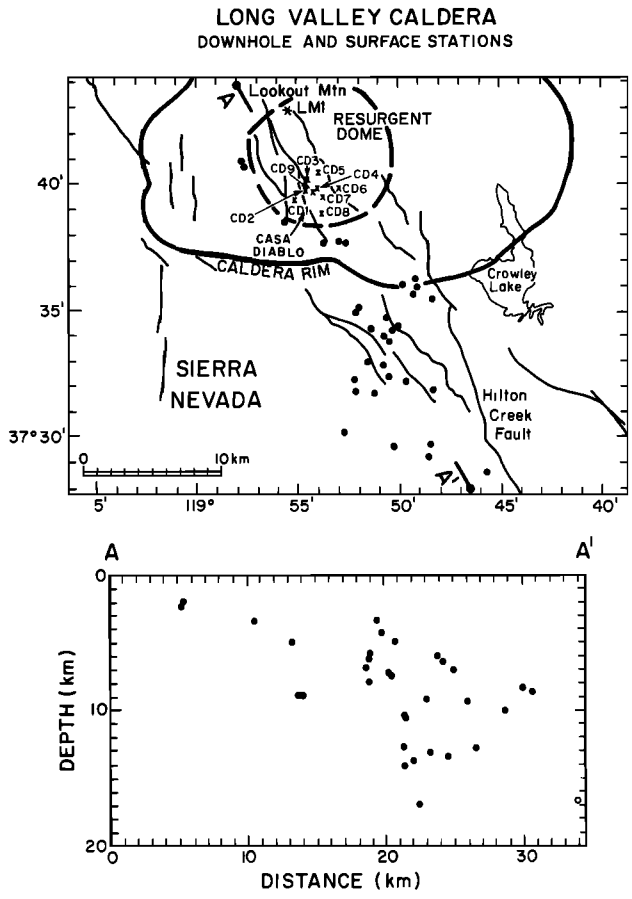

Fig. 1. (Top) Map of the Long Valley caldera and surrounding region. The borehole station (LM1) was located just south of Lookout Mountain. Surface stations (CD1-CD9) were deployed in the Casa Diablo area above the proposed magma chamber identified by Sanders [1984]). Earthquakes (relocated with HYPOINVERSE; see also Table 1) recorded by the downhole station and some of the surface stations are shown as solid circles. (Bottom) a north-northwest striking cross section showing depth distribution of hypocenters.

shallow crustal depths [e.g., Savage and Clarke, 1982; Rundle and Whitcomb, 1984; Savage et al. 1987].

In this study the high-quality downhole data from the 900-m-deep borehole are emphasized. The downhole data have a high signal to noise ratio, since the background noise level is 18-24 dB less at 900-m depth than at the surface. Furthermore, the downhole seismograms are simpler (with clear P and S waves) than surface seismograms because the near-surface caldera fill strongly attenuates or scatters the primary P and S waves.

Data Analysis

The borehole (LM1) is located 2.2 km southeast of Lookout Mountain (37° 42.98' and 118° 55.64') and approximately 7 km to the north of the Casa Diablo area (Figure 1). The downhole package was deployed at 900-m depth and contained an 8-Hz three-component seismometer assembly (Mark Products model L-28 LA). The package at the bottom of the borehole at 900-m depth rested in place on its own weight. A layer of dense residual drilling mud provided good coupling to the bottom of the borehole. The waveform data were recorded by a Sprengnether DR-100 digital recorder at a sampling rate of 100 samples per second. The DR-100 recorder was operated in event-triggered mode based on short- and long-term signal averages. A comparison of the P amplitudes recorded by the vertical and the two horizontal components suggests that the first horizontal component is oriented approximately north-south and the second horizontal component is oriented approximately east-west. For earthquakes located to the south of the downhole station, the first and second horizontal components are therefore radial and transverse components, respectively.

The downhole station and a temporary 13-station surface network were operated from September 19 to October 10, 1984. The surface stations were deployed in two clusters, four stations around the borehole and nine stations tightly clustered (average spacing 0.5-1.0 km) in the Casa Diablo area (Figure 1). All of the surface stations had a 4.5-Hz three-component seismometer (Mark-Products model L-1B) and a DR-100 digital recorder. During the field experiment, approximately 200 local earthquakes were recorded by four or more stations, but for this study, only earthquakes recorded by both the downhole station (LM1) and seven surface stations are examined. Only the stations in the Casa Diablo area that recorded data used in this study are plotted in Figure 1.

Independently recorded P and S arrival time data, first-motion polarities, magnitudes, and hypocentral parameters from the RTP (real time processor) were made available by the U.S. Geological Survey (R. Cockerham, written communication, 1984). P and S arrival time data and first-motion polarities from the CUSP (CIT/USGS seismic processing) system were also made available by the U.S. Geological Survey (S. Stewart and R. Dollar, written communication, 1986). These data made it possible to use the USGS seismographic network as an independent network to calculate origin time, location, and depth of each earthquake. The computer program HYPOINVERSE [Klein, 1985] was used to recalculate the origin time, location, and depth (Table 1) using the standard station delays and velocity model for the Long Valley region [Cockerham and Pitt, 1984]. In three cases, time corrections that were determined using a portable master clock were required to maintain the same time reference for the USGS and the DR-100 data (see Tables 1 and 2).

Initially, the P and S arrivals were picked graphically from a computer terminal to an accuracy of 0.01 s using an interactive graphics program. Travel time residuals that were calculated for the temporary stations did not contribute to the calculation of the origin time and hypocenter. HYPOINVERSE was also used to calculate distances and travel times from the downhole or surface stations to the epicenters to facilitate plotting of reduced travel times

TABLE 1. Relocated Hypocenters of Earthquakes in Long Valley Recorded by the Downhole Instrument (LM1)

Date	Origin Time	Latitude	Longitude	Depth Km	Relative Amplitudes at (LM1) PV	SV	PR	SR	SH	Coda	Remark
Sept. 21, 1984	1346:19.7	37°-34.4	118°-50.0	12.7	10	33	8	41	51	10	1
	1347:19.6	37°-34.4	118°-50.0	12.8	9	20	5	28	30	8	1
	1350:50.3	37°-34.4	118°-50.0	12.5	9	27	6	52	36	11	1
	1351:10.7	37°-39.6	118°-46.5	9.8	3	33	2	44	44	11	1
Sept. 23, 1984	1451:53.6	37°-34.7	118°-50.7	7.4	18	22	16	38	30	11	1
Sept. 27, 1984	2214:45.1	37°-32.5	118°-49.9	8.9	51	13	38	22	22	16	
	2241:13.4	37°-33.9	118°-50.7	10.4	21	31	14	42	42	10	
Sept. 28, 1984	0150:0.6	37°-35.3	118°-52.1	6.5	17	39	12	58	68	14	
	0313:6.9	37°-32.4	118°-50.5	7.8	35	34	28	40	46	11	
	0532:19.1	37°-31.8	118°-52.1	6.0	9	37	6	58	68	22	
	0924:8.1	37°-36.2	118°-49.2	5.6	32	26	26	46	34	11	
	1551:54.3	37°-33.9	118°-50.7	10.6	51	29	32	54	52	21	
	2119:20.2	37°-35.5	118°-48.3	4.9	31	35	28	60	78	20	
Sept. 29, 1984	0310:50.9	37°-33.0	118°-51.5	16.9	28	41	16	82	88	18	
	0454:35.1	37°-34.3	118°-51.4	7.4	46	34	38	42	46	15	
	0515:17.7	37°-38.5	118°-55.6	3.4	8	34	6	28	68	15	
	1402:48.7	37°-40.8	118°-57.7	2.0	24	35	14	22	46	17	
	1403:59.0	37°-40.7	118°-57.8	2.1	19	33	12	22	52	16	
	2106:27.8	37°-28.6	118°-45.7	16.9	31	16	22	18	16	8	
Sept. 30, 1984	0103:6.0	37°-37.7	118°-52.6	8.8	27	54	18	70	38	23	
	0240:30.2	37°-29.1	118°-48.6	8.6	35	20	34	28	42	10	
	1057:22.7	37°-29.6	118°-50.2	10.0	48	11	39	18	16	5	
Oct. 4, 1984	1033:27.3	37°-29.4	118°-48.6	9.5	40	22	30	23	23	14	
	1122:48.3	37°-35.2	118°-52.1	6.9	22	24	11	47	33	11	
	1738:34.4	37°-33.0	118°-51.0	12.2	51	18	37	24	38	10	
	1944:9.0	37°-38.4	118°-53.0	8.4	17	34	9	36	39	7	
Oct. 6, 1984	0028:54.8	37°-32.3	118°-52.1	9.2	10	26	7	36	26	8	2
	0244:9.1	37°-30.4	118°-52.5	8.8	20	26	9	36	37	14	2
	0855:59.6	37°-31.9	118°-48.2	14.0							2,4
	1250:51.7	37°-37.9	118°-53.7	4.8	31	25	19	31	29	16	2
Oct. 7, 1984	1307:35.1	37°-36.0	118°-49.8	7.9	8	28	6	32	26	15	3
	1450:2.8	37°-36.3	118°-49.1	6.4	36	28	25	28	36	12	3
	2355:40.9	37°-35.9	118°-49.3	5.0	25	35	18	32	28	14	3

1, Time correction of -1.0 s applied to all stations; 2, time correction of -3.3 s applied to station LM1; 3, time correction of -0.3 s applied to station LM1; 4, S wave not recorded at station LM1 due to short trigger.

TABLE 2. Hypocenters of Long Valley Earthquakes

Date	Origin Time	Latitude	Longitude	Depth Km	Travel Time,s		Diff-	Epicentral Distance, km		Remark
					Observed	Calculated	erence	1986	This Study	
Sept. 21, 1984	1346:19.7	37°-34.4	118°-50.1	15.0	3.95	3.98	-0.03	16.7	17.9	1
Sept. 27, 1984	2214:45.2	37°-32.1	118°-49.7	8.5	4.14	4.17	-0.03	21.4	22.0	
	2241:13.4	37°-33.6	118°-50.9	11.6	3.80	3.82	-0.02	18.0	18.8	
Sept. 28, 1984	0150:0.6	37°-34.9	118°-52.2	7.6	3.05	3.14	-0.09	14.6	15.9	
	0313:6.9	37°-32.2	118°-50.6	8.0	4.07	4.03	0.04	21.2	21.3	
	0532:19.1	37°-31.8	118°-52.1	7.3	4.08	4.03	0.05	20.8	21.4	
	0924:8.0	37°-36.2	118°-48.8	2.7	3.23	3.09	0.14	17.1	16.0	
	1551:54.2	37°-33.7	118°-51.0	12.9	3.88	3.87	0.01	18.0	18.5	
	2119:20.2	37°-35.4	118°-48.2	6.9	3.39	3.43	-0.04	19.1	17.8	
Sept. 29, 1984	0454:35.4	37°-34.9	118°-50.6	5.8	3.01	3.23	-0.22	17.4	16.8	
	0515:17.7	37°-38.5	118°-55.6	4.7	1.88	1.77	0.11	7.7	8.3	
Sept. 30, 1984	0103:6.0	37°-37.7	118°-52.6	10.2	2.55	2.56	-0.01	9.8	10.8	
	0240:30.3	37°-29.3	118°-48.6	8.7	5.15	5.06	0.09	28.3	27.4	
	1057:22.6	37°-29.6	118°-50.2	11.6	4.90	4.95	-0.05	25.4	26.1	
Oct. 4, 1984	1033:27.4	37°-29.6	118°-48.5	9.7	5.01	5.00	0.01	27.0	26.9	
	1122:48.3	37°-35.2	118°-52.1	8.2	3.12	3.07	0.05	14.9	15.3	
	1738:34.6	37°-32.8	118°-50.6	10.4	3.91	3.97	-0.06	19.5	20.3	
Oct. 6, 1984	0855:59.7	37°-31.9	118°-48.2	14.0	4.64	4.65	-0.01	22.3	23.3	2
	1250:51.7	37°-37.7	118°-53.5	5.6	2.11	2.13	-0.02	11.8	10.2	2

These events were also analyzed by Elbring and Rundle [1986].
1, Time correction of -1.0 s applied to all stations; 2, time correlation of -3.3 s applied to station LM1.
Observed travel time is from hypocenter to station LM1; calculated travel time is from hypocenter to station LM1 using velocity model from Cockerham and Pitt [1984]; difference is between observed and calculated travel times; epicentral distances are those used by Elbring andd Rundle [1986] and those determined in this study using HYPOINVERSE.

or S travel times divided by P travel times versus hypocentral depth.

P, S, and coda amplitudes were measured from paper playback seismograms (Table 1). The coda amplitudes were measured 10 s after the origin time of the earthquake and averaged over a 1-s interval and three components, which are labeled CZ, CR, and CT in Figure 2. Most of the earthquakes had S-P times of 1.5 to 4 s. The P amplitude was determined as $P = \sqrt{PZ^2 + PR^2}$, where PZ and PR are the largest peak-to-peak P (arriving within 0.5 s of the P wave) on the vertical and radial components, respectively (Figure 2). The SV amplitude was determined similarly as $SV = \sqrt{SZ^2 + SR^2}$, where SZ and SR are the peak-to-peak S amplitude (arriving within 0.5 s of the S wave) on the vertical and radial component, respectively. The SH amplitude was simply the largest peak-to-peak amplitude from the transverse component (ST). The P and S amplitudes were normalized with the respective coda amplitudes to establish whether P or S amplitudes were changing relative to the coda. The codas of all earthquakes in the data set were similar in character and amplitude, in part because of the limited magnitude range (1.0-2.0) of the earthquakes.

Results

This study consists of three independent attempts to identify evidence for a magma chamber in the downhole and surface seismograms. These attempts are (1) a search for S wave shadowing, (2) a search for travel time delays in the downhole data previously reported by Elbring and Rundle [1986], and (3) a search for travel time delays by comparing the surface and downhole data.

Search for S Wave Shadowing

The attenuation of S waves is affected by the background or regional crustal Q as well as by localized zones of low Q that may result in S wave shadowing. Several of the downhole seismograms showed S amplitudes that are significantly reduced in comparison to the respective P amplitudes. Sample seismograms of an earthquake with normal S amplitudes (S amplitude greater than P amplitude) and an earthquake with anomalously small S amplitudes (S amplitude less than P amplitude) are shown in Figure 2. These small S amplitudes were originally interpreted by the author to represent S wave shadowing and possibly to result from a shallow crustal magma chamber.

Displacement spectra of the S waves have similar shape for most of the downhole seismograms. Because the absolute spectra level varies depending on the peak-to-peak amplitude of the waveform, it seemed appropriate to use the maximum peak-to-peak amplitude as a measure of the signal strength. The P, S, and coda amplitudes are listed in Table 1. Both the P and S amplitudes were normalized with respect to the coda amplitude of the respective trace before plotting in Figure 3. The coda have similar frequency content and show a similar amplitude decay for all of the downhole seismograms. The normalization to coda

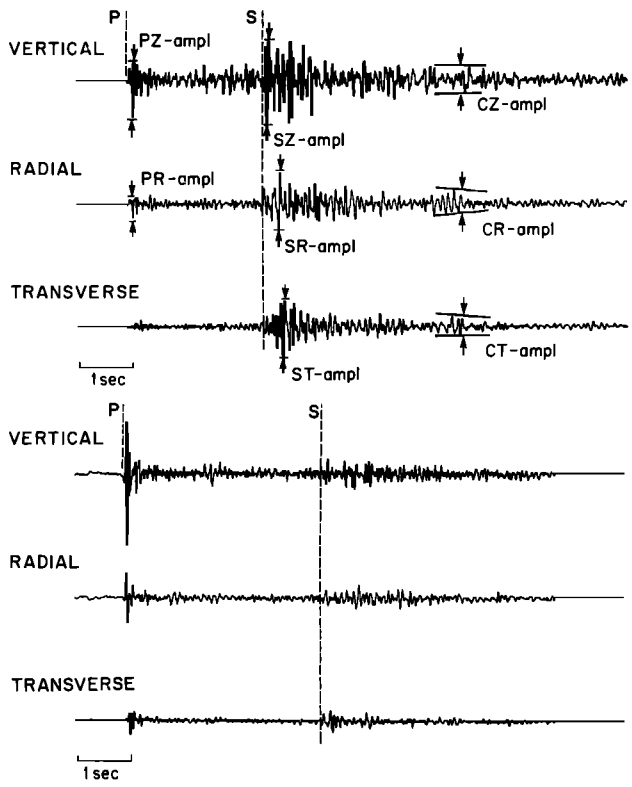

Fig. 2. Sample seismograms from the downhole three-component seismometer at 900-m depth. (Top) Seismograms with normal S waves. Labeling of P, S, and coda amplitudes shows how these are measured. PZ and PR are vertical and radial component P wave amplitudes, respectively. SZ, SR, and ST are vertical, radial and transverse component S wave amplitudes, respectively. CZ, CR, and CT are vertical, radial, and transverse component coda amplitudes, respectively. Dashed vertical lines indicate direct P and S arrivals. (Bottom) Seismograms with low S amplitudes as compared with the P amplitude.

amplitude was chosen because the coda represents an average attenuation effect over a much larger crustal volume and an average radiation pattern effect over all directions [Aki, 1982]. The normalization makes it possible to evaluate whether the P amplitude increased, and hence the S amplitude appears to be small, or if the P amplitude is unchanged and the S amplitude actually decreased. In Figure 3 the seven earthquakes that have P amplitudes greater than SV and SH amplitudes (represented by open circles and labeled with the hour and minute of the origin time of the earthquake) were considered to show S wave shadowing. A line with a slope of 1.0 is plotted for reference in Figure 3. In most cases where the P amplitude is greater than the S amplitude, suggesting possible S wave shadowing, the P amplitude has increased and the S amplitudes remain approximately the same size. Most of these earthquakes are located 20-30 km to the south of the downhole station.

In general the S amplitude can be 5 times larger than the P amplitude because the

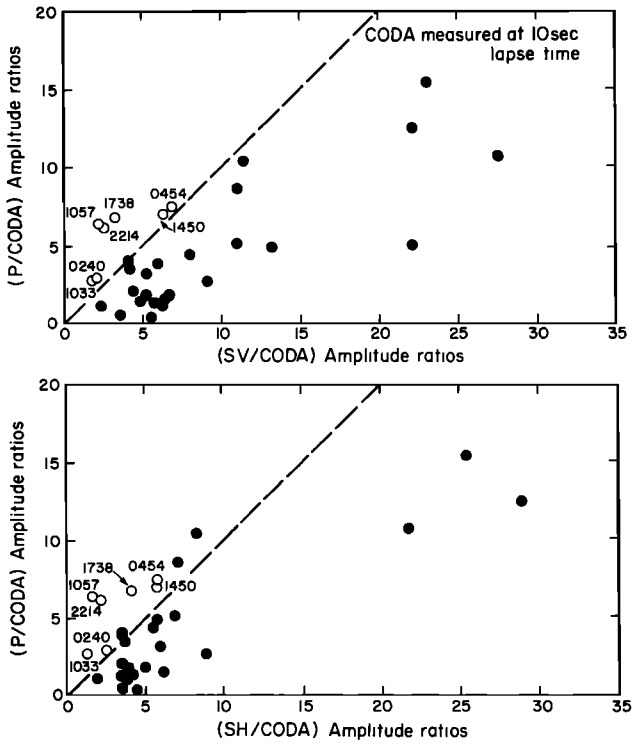

Fig. 3. (Top) P amplitude versus SV amplitude where both are normalized to the coda amplitude measured 10 s after the origin time of the earthquake. The reference line has a slope of 1.0. The four events with large S amplitudes are located closest to the borehole. (Bottom) Amplitude normalized to the coda amplitude. Seven earthquakes that have larger P amplitudes than both SV and SH amplitudes are considered to have strongly attenuated S waves. These are plotted as open circles and labeled with the hour and minute of the origin time of the earthquake (see also Figures 4 and 6 and Table 1).

amplitude ratio is proportional to $(Vp/Vs)^3$, where Vp is the P velocity and Vs is the S velocity [Aki and Richards, 1980]. The SV/P and SH/P amplitude ratios, however, also vary depending on the focal mechanism or the azimuth and takeoff angle of the ray traveling to the station recording the earthquake. To evaluate the radiation pattern effect on the observed SV/P and SH/P amplitude ratios, the lower-hemisphere focal mechanism for each earthquake was determined using the grid-searching algorithm FPFIT [Reasenberg and Oppenheimer, 1985]. The focal mechanisms for the seven events with low SV/P and SH/P ratios are plotted in Figure 4 and labeled with the date, hour, and minute of the origin time of each earthquake (Table 1). Because most of the earthquakes have only a few first-motion polarities available, the algorithm FPFIT can fit more than one focal mechanism to the data from each event. These multiple mechanisms for each earthquake are also plotted, but flagged by a star, in Figure 4. In most cases the ray traveling to the downhole station (LM1) has a subhorizontal takeoff angle (85-120°) with an azimuth 10-30° west of north.

Because all of the events are of small magnitude (M<2.0), the number of available first-motion polarities is limited. At least five of the seven events, however, would satisfy a strike-slip mechanism similar to the first mechanism shown in the upper left-hand corner of Figure 4. Because of the uncertainty in the determination of fault plane solutions and the orientation of the downhole seismometers, it is only possible to carry out a qualitative comparison between the observed and theoretically predicted amplitude ratios.

Theoretical radiation patterns for the SV/P and SH/P ratios are shown in Figure 5 for a double couple in a uniform half-space [Aki and Richards, 1980]. This strike-slip mechanism, which is similar to the first mechanism in Figure 4 with one nodal plane striking N30°E, was chosen because the majority of earthquakes occurring west of the Hilton Creek fault have strike-slip mechanisms with one nodal plane

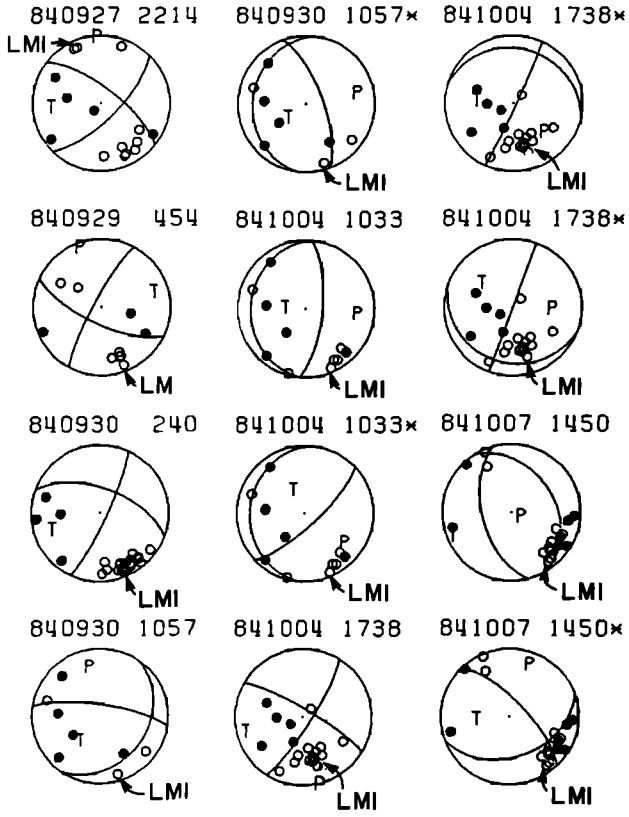

Fig. 4. Focal mechanisms of the seven earthquakes (Figure 3) that have larger P amplitude than SV and SH amplitudes. Each solution is labeled with the date, hour, and minute of the origin time of the earthquake. The same hour and minute are also used for labeling in Figures 3 and 6. Multiple focal mechanisms for the same earthquake are flagged by a star, and nodal planes are determined using the grid-search algorithm by Reasenberg and Oppenheimer [1985]. Open circle indicates first-motion polarity up or compressional, and solid circle indicates down or dilational. The first-motion polarity of the borehole station (LM1) is labeled.

striking N10°E-N30°E (R. Cockerham, personal communication, 1987). No free-surface correction is needed because the seismometer is deployed in a 900-m-deep borehole. Because both P and SV waves have identical azimuthal radiation patterns for a strike-slip mechanism, the SV/P radiation pattern is independent of azimuth. The P amplitude, however, increases from a small value (<0.01) for nearly vertical takeoff angles to a value of approximately 1.0 for nearly horizontal takeoff angles. Hence the SV/P ratio is less than 1.0 for subhorizontal takeoff angles and all azimuths. The SH/P ratio varies with azimuth and is less than 1.0 for azimuths that are at a 45°±5° orientation relative to the P nodal planes. One of these nodal planes of SH/P ratio coincides with the azimuth between the downhole seismometer and most of the hypocenters. If the two radiation patterns of SV/P and SH/P ratio in Figure 5 are superimposed, the three nodal points (B, P, and T axis) of total S wave motion become apparent. One of these nodes (P axis) has a similar azimuth as the azimuth of the SH/P nodal plane from the hypocenters to the borehole.

Although most of the focal mechanisms are not well constrained, some may have a significant dip-slip component of motion. In such cases the radiation patterns become more complex, and theoretical SV/P and SH/P ratios need to be calculated for each event. If the dip-slip component is small, as for instance, in the second focal mechanism in Figure 4, both the SV/P and SH/P ratios become greater than 1.0 in the immediate vicinity of the nodal planes as the P amplitude becomes nodal. This may make it difficult to observe S wave shadowing along approximately north-south paths because many of the focal mechanisms have one nodal plane oriented approximately north-south.

The hypocenters of the earthquakes showing low SV/P and SH/P ratios are shown as open circles in Figure 6. The calculated radiation patterns indicate that the observed variations in P and S amplitudes are in part caused by radiation pattern effects. The near colocation of earthquakes with normal amplitude ratios versus small ratios also suggests that the observed variation in amplitude is an artifact caused by the radiation pattern. The relative position of the hypocenters and the proposed magma chamber by Sanders [1984] in Figure 6 shows that several of the P and S waves should pass through or at least grace the zone of high S wave attenuation delineated in that study. The results of this study, however, indicate that both P and S amplitudes vary relative to coda amplitude. All of the seven seismograms that were thought to have anomalously low S amplitudes, can be explained in terms of radiation pattern. Hence there is no conclusive evidence for shadowing or anomalous attenuation of S waves in the downhole seismograms.

Search for Travel Time Delays

If the proposed magma chamber has a large spatial extent, it is possible that it is associated with a significant travel time delay for both P and S waves. To show that travel time delays exist, Elbring and Rundle [1986]

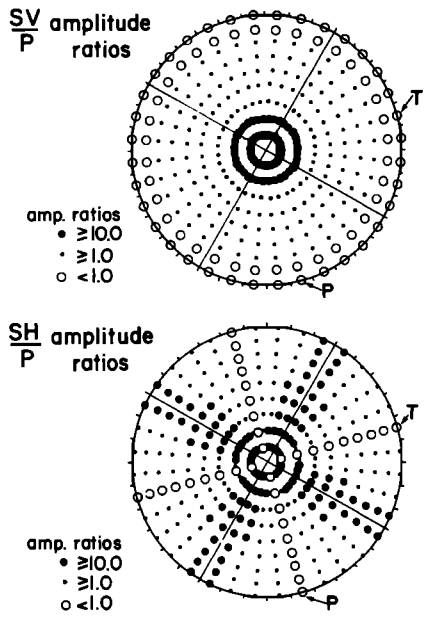

Fig. 5. Calculated radiation pattern plotted on a lower-hemisphere stereographic projection for a double couple with moment in a homogeneous half-space [Aki and Richards, 1980]. (Top) The calculated SV/P amplitude ratio for a typical strike-slip focal mechanism. Solid circle indicates that the SV/P ratio is greater or equal to 1.0. Open circle indicates that the SV/P ratio is less than one. (Bottom) The calculated SH/P amplitude ratio for the same mechanism. Solid circle indicates SH/P > 1.0, and open circle indicates SH/P < 1.0.

used a subset of the downhole data analyzed in this study (see Table 2 and Figure 7). They plotted a record section of reduced travel time (using a reduction velocity of 6.0 km/s and slant distance as reducing distance) as a function of hypocentral depth (Figure 8). The velocity model shown on top in Figure 8 is the velocity model (including the low-velocity wedge below the Casa Diablo area) inferred by Elbring and Rundle [1986] by fitting the first arrivals and some of the secondary arrivals in the record section. The low-velocity wedge is derived from the following observation made by Elbring and Rundle [1986]: "In Figure 8, below 7 km the first arrivals in the record section are consistently delayed by as much as 0.4 s when compared to first arrivals in the depth range between 5 and 7 km." Using forward modeling by trial and error, they concluded that the low-velocity wedge was needed to satisfy these first arrivals.

To evaluate the applicability of the Elbring and Rundle [1986] method to data recorded by both downhole and surface stations, several tests have been made. First, an evaluation of the appropriate reduction velocity was carried out. Second, the observed and the calculated travel times for a flat layered model are compared. Third, the epicentral distances between the borehole station and the hypocenters from Elbring and Rundle [1986] and recalculated

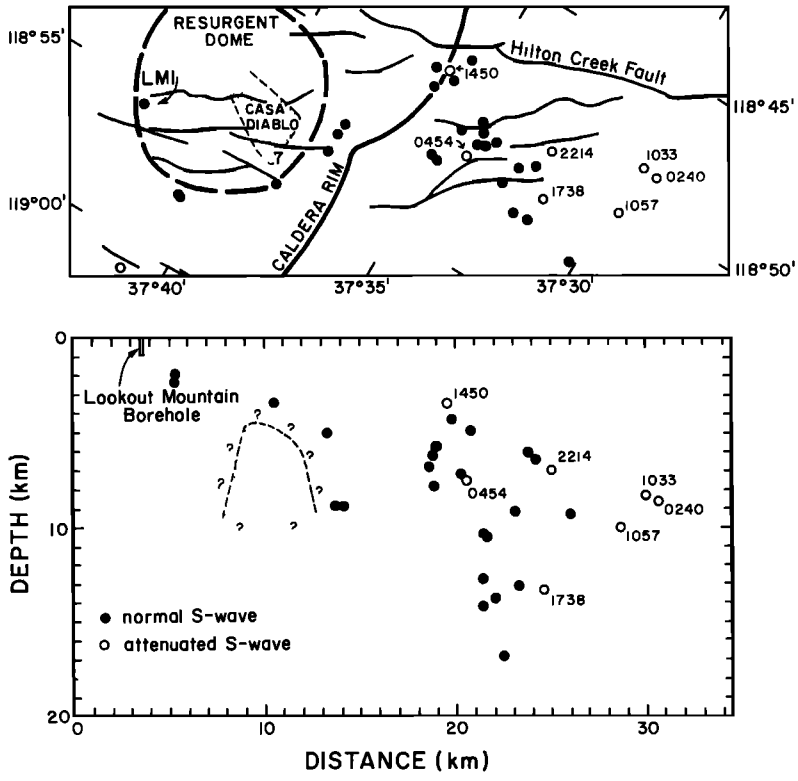

Fig. 6. (Top) Map of epicenters of earthquakes recorded by the borehole station (LM1). Solid circles represent earthquakes with regular S amplitudes. Open circles (labeled with hour and minutes of the origin time) represent earthquakes that have P amplitude greater than SV and SH amplitudes. Shaded area in Casa Diablo indicates the 7-km depth contour of the proposed magma chamber from Sanders [1984]. (Bottom) A cross section showing hypocenters and an approximate outline of the proposed magma body from Sanders [1984].

distances from HYPOINVERSE are compared. Fourth, to test for possible variations in the Vp/Vs ratio from 1.67 to 1.9 (as suggested by Elbring and Rundle [986]), the ts/tp ratio (where tp and ts are the observed P and S travel times, respectively) for each event was plotted as a function of depth. The results of these tests are discussed next.

The crustal structure of the Long Valley caldera has been studied extensively [e.g. Hill et al., 1985; Kissling et al., 1984; Cockerham and Pitt, 1984]. The velocity model used routinely for earthquake locations in the Long Valley area by the U.S. Geological Survey (e.g., Cockerham and Pitt [1984]; this model is also included in Figure 9) that is based on these studies can be used to determine the appropriate reduction velocity. The program HYPOINVERSE was used to calculate travel times through this model from three sets of hypothetical sources located 10, 20, and 30 km away from the borehole station (Figure 9). Each set consists of 29 sources at 0.5-km intervals over the depth range from 1.0 to 15.0 km. The travel times are plotted with three different reduction velocities (5.7, 6.0, and 6.3 km/s) in the top half of Figure 9. The results show that the 5.7-km/s reduction velocity is more appropriate for the Elbring and Rundle approach than the 6.0 km/s for the range of epicentral distances (10-30 km). Using the higher reduction velocity of 6.0 km/s, Elbring and Rundle [1986] introduce a focal depth dependent spread in the first arrivals of up to 0.25 s.

As an initial test for the presence of large P wave travel time delays, the difference between observed and calculated travel times is listed in Table 2 and plotted as a function of focal depth in Figure 10. The calculated travel times were obtained by using the flat layered velocity model for the Long Valley region [Cockerham and Pitt, 1984]. The only significant variation in the travel time difference is the early arrival by 0.2 s from an earthquake at 5.9-km depth. No systematic delay in arrivals can be seen as a function of focal depth.

To obtain the reduced travel time curve in Figure 10, the slant distance between the downhole seismometer and the hypocenter has to be calculated. The slant distance is defined as $\sqrt{D^2+Z^2}$, where D is the epicentral distance and Z is the hypocentral depth. In this study, HYPOINVERSE was used to calculate the epicentral distance using the fixed hypocentral parameters (including depth) published by Elbring and Rundle [1986] and initially provided by the U.S. Geological Survey (R. Cockerham, written communication, 1984). The travel times were determined as the difference between the picked

P arrival time and the respective origin time published by Elbring and Rundle [1986]. The reduced travel time versus depth profile from this study and from Elbring and Rundle [1986] are plotted in Figure 10 at a reduction velocity of 6.0 km/s. The same profile from this study is also plotted at reduction velocities of 5.7 and 6.3 km/s in Figure 10. The first arrivals below 7 km are not delayed with respect to the first arrivals above 7-km depth, in contrast to the suggestion by Elbring and Rundle [1986]. In addition, the reduction velocity of 5.7 km appears to provide a somewhat smoother curve in the depth range of 3 to 10 km. The effect of the choice of reduction velocity, however, appears to be small and does not explain the substantial difference between the reduced travel time of Elbring and Rundle [1986] and this study.

In an attempt to explain this difference in reduced travel times, the epicentral distances used by Elbring and Rundle were redetermined from the following information: (1) the P arrival times in the reduced travel time

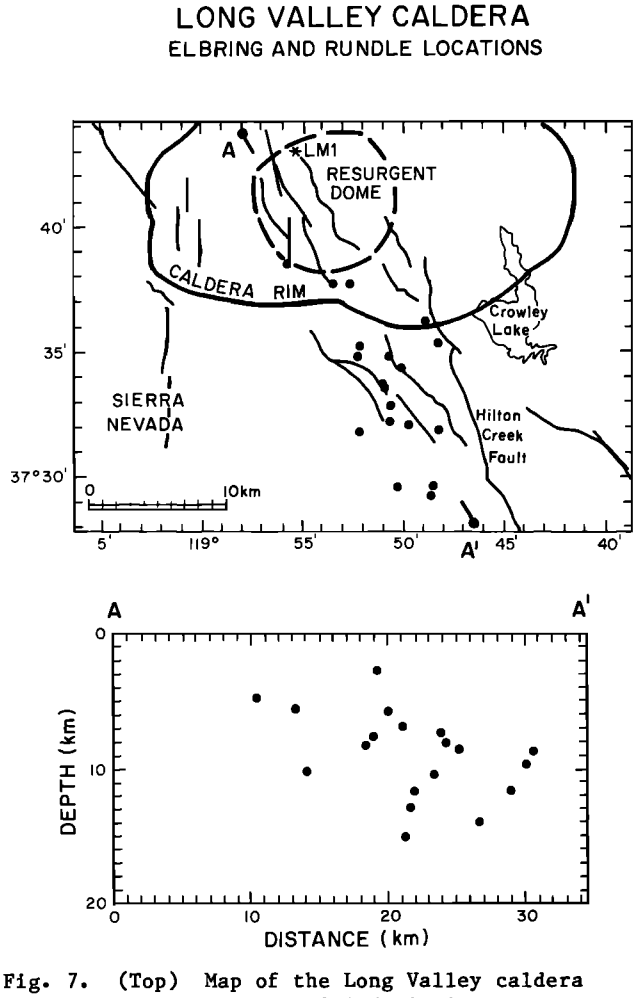

Fig. 7. (Top) Map of the Long Valley caldera and surrounding region. Solid circles represents 19 epicenters of local earthquakes published by Elbring and Rundle [1986]. (Bottom) A north-northwest cross section showing depth distribution of hypocenters.

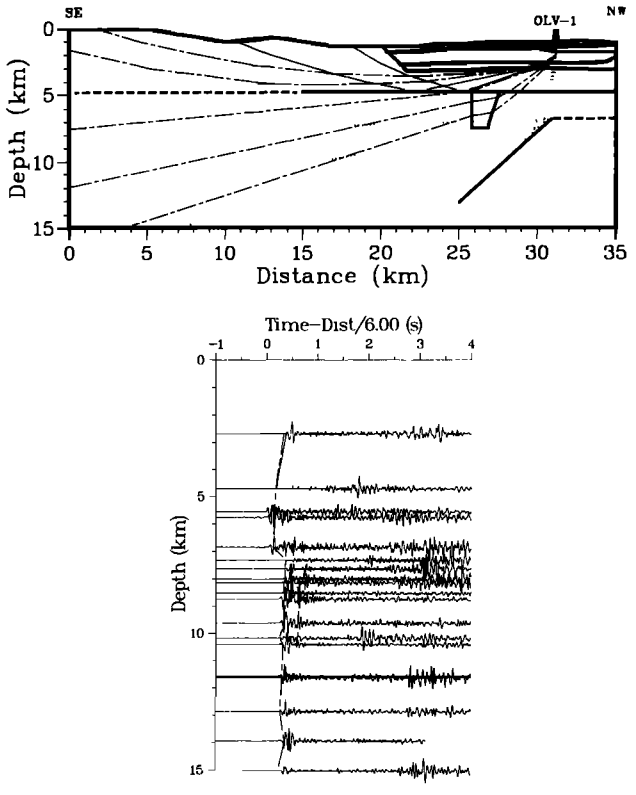

Fig. 8. (Top) Crustal model showing low-velocity wedge at a 5-8 km depth to the southeast of the borehole OLV-1 (in this study labeled LM1). Also shown are ray paths used to derive this model. (Bottom) reduced travel time record section as a function of depth. Note how three P waves in the depth range 5-7 km arrive 0.4 s earlier than all the others [from Elbring and Rundle, 1986, Figure 4].

curve in Figure 8 [from Elbring and Rundle, 1986], (2) the travel times used in this study, which are the difference between the observed P arrival and the origin time published by Elbring and Rundle [1986], and (3) hypocentral depth published by Elbring and Rundle [1986]. The differences between the Elbring and Rundle epicentral distances and the epicentral distances calculated with HYPOINVERSE (doing only one iteration step with the same fixed location) are listed in Table 2 and plotted in Figure 11. This depth profile has a shape similar to the reduced travel time profile from Elbring and Rundle [1986] and provides a simple explanation for the shape of the travel time curve reported by Elbring and Rundle [1986] (Figure 10).

Elbring and Rundle [1986] constructed similar reduced travel time versus depth profiles for S waves. They concluded from trial and error forward modeling of the S arrivals using ray tracing that the Vp/Vs ratio was 1.67 in the upper crust with the exception of the low-velocity wedge, where they found a Vp/Vs ratio of 1.9. To test their findings of possible variations in the Vp/Vs ratio, the observed ratio of S to P travel times for each earthquake are plotted as a function of depth in

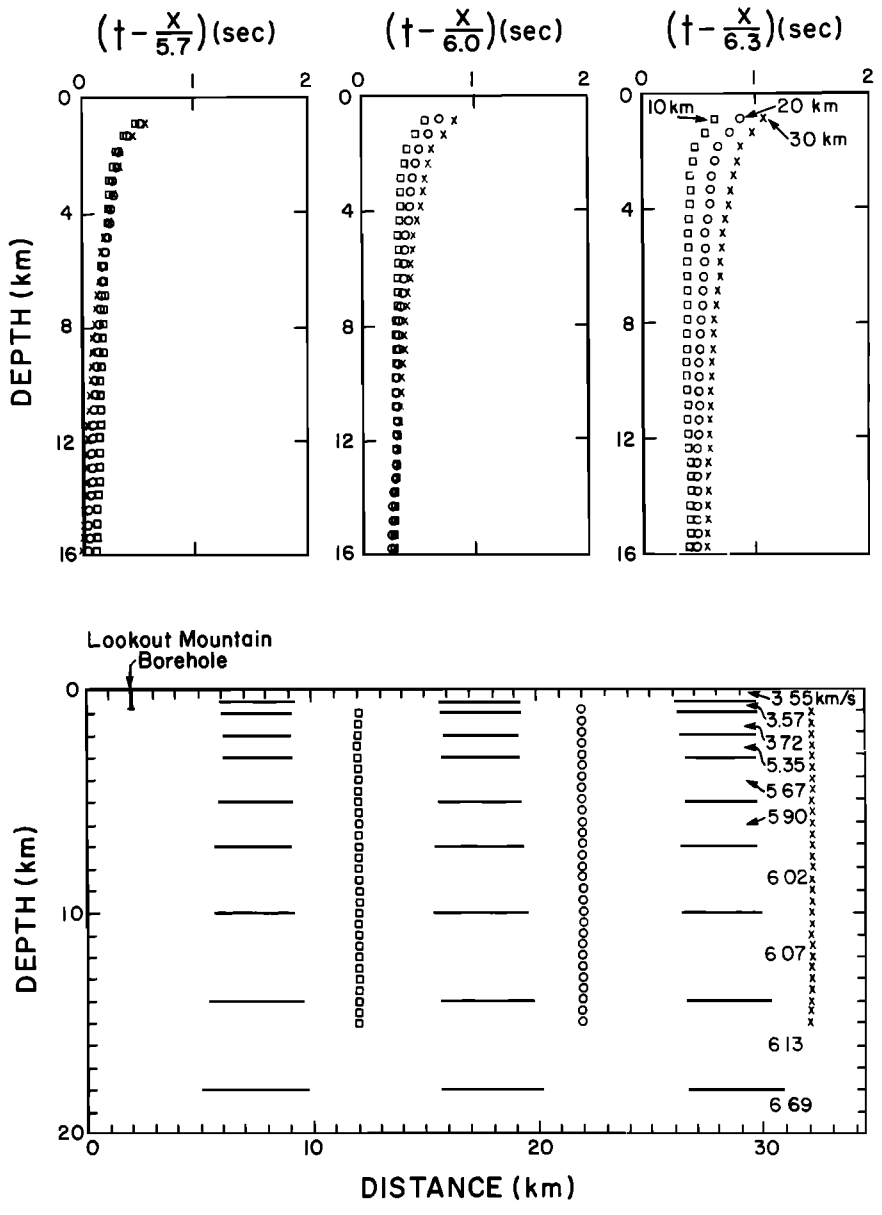

Fig. 9. Calculated reduced travel time as a function of depth. Fixed sources are assumed at 10, 20, and 30 km distance away from the borehole site, and HYPOINVERSE is used to calculate travel times and epicentral distances. Crustal velocity model is from Cockerham and Pitt [1984]. Note how different reduction velocities affect the relative arrival times.

Figure 12. The uncertainty in determining P and S travel times is approximately 0.1 s, and the uncertainty in depth determination is ±1 km in most cases. The data in Figure 12 illustrate the absence of significant variations of the Vp/Vs ratio with depth.

The values from the Elbring and Rundle [1986] study are also shown for comparison in Figure 12. Because the average total ray path may be 20 km long and only a 3-km-long section of the ray path would be within the low velocity wedge, the average change in S travel time caused by the high Vp/Vs ratio within the wedge would be approximately 0.2 s. In the depth range 5-8 km the Vp/Vs ratio (averaged over a 20-km distance) therefore increases from 1.67 to 1.72 because of the high Vp/Vs within the low-velocity wedge. It thus follows that the downhole data cannot easily resolve the variation in the Vp/Vs ratio in the low-velocity wedge.

Search for Travel Time Delays: Comparison of Surface and Downhole Data

To compare the difference between observed and calculated travel times versus depth profiles for both downhole and surface stations, a data set of 32 earthquakes was analyzed (see Figure 1 and Table 1). The hypocenters and travel times were recalculated using HYPOINVERSE

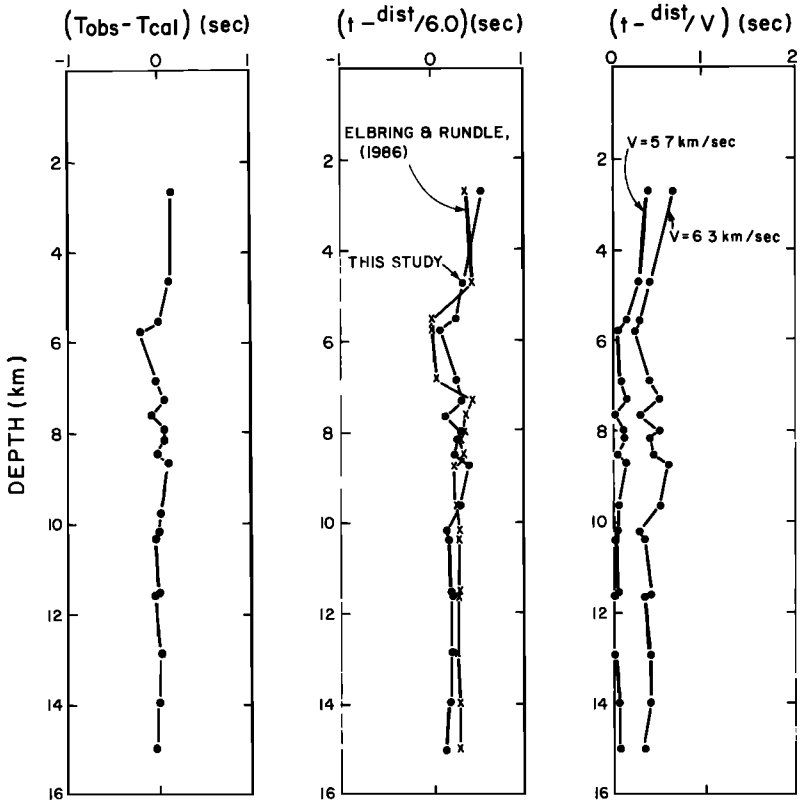

Fig. 10. (Left) Difference between observed and calculated travel time plotted as a function of focal depth. (Center) A comparison of reduced travel time versus focal depth from Elbring and Rundle [1986] and from this study. (Right) Data from this study plotted at different reduction velocities. Only data from the 19 events studied by Elbring and Rundle [1986] are included.

with the U.S. Geological Survey arrival time data and corresponding velocity model with station delays. Arrival time data from the temporary downhole and surface stations were intentionally not included in determination of the respective hypocenter. Hence the hypocenters determined by HYPOINVERSE are almost identical to the hypocenters provided by the U.S. Geological Survey. The surface stations CD1 through CD9 were deployed on top of the proposed magma chamber [Sanders, 1984] in the Casa Diablo area (Figure 1). Because the downhole station is located 7 km to the north of the surface stations, it is possible that the profiles for these stations are different. In particular, a low-velocity body beneath the Casa Diablo area would be expected to have a greater influence on the deeper traveling rays recorded by the downhole station.

The profiles of the difference between observed and calculated travel times for both downhole and surface stations are plotted as a function of focal depth in Figure 13. Stations CD3, CD5, and CD6 are located on the north side of the Casa Diablo area, while CD1, CD4, CD9, and CD7 form an east-west profile across the center of the Casa Diablo area. Stations CD2 and CD8 are not included because they recorded only a few of these earthquakes. Neither the downhole nor the surface station profiles show systematic travel time delays as a function of focal depth. The downhole and surface station data therefore do not require a low-velocity body at shallow crustal depths below the Casa Diablo area or to the south beneath the south moat area.

Comparing the Vp/Vs ratios observed for travel paths to the borehole and surface stations located in the Casa Diablo area (Figure 14) shows that all the stations have a fairly constant Vp/Vs ratio with depth. The data from the surface stations have greater scatter because the onset of the S wave may be obscured by near-surface S to P converted phases. The downhole data resolve smaller variations in the Vp/Vs ratio as a function of depth. The absence of systematic variations with depth in the Vp/Vs ratio for both the downhole and surface data suggests that these data cannot resolve a magma chamber beneath Casa Diablo as small as that proposed by Elbring and Rundle [1986].

Discussion

The seismograms from the downhole instrument placed at 900-m depth are some of the highest quality seismograms ever collected within the Long Valley caldera. They were specifically collected to gather detailed evidence about a possible magma chamber beneath the Long Valley

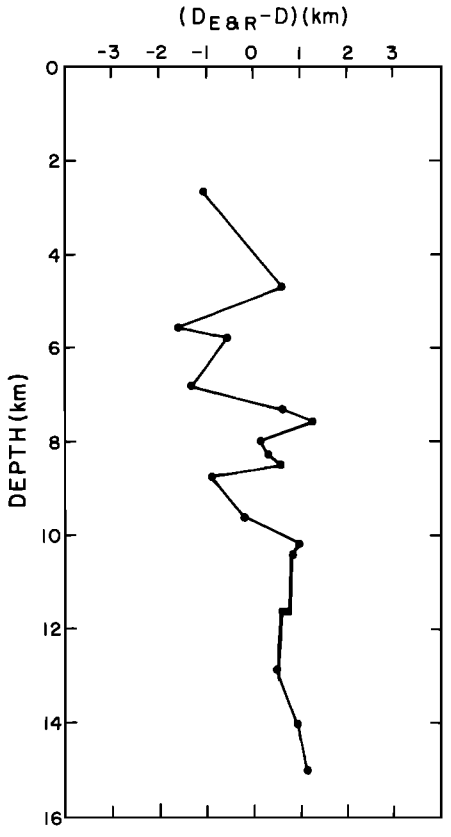

Fig. 11. Difference in epicentral distance used by Elbring and Rundle [1986] and the epicentral distance calculated by HYPOINVERSE for the same hypocenters and the same borehole station location.

caldera [e.g., Sanders, 1984]. It is thus disappointing to discover the absence of evidence for a magma chamber in the downhole seismograms. This negative result does not appear to be from artifacts in the data but is rather a fundamental observation.

The failure of the borehole experiment to provide clear evidence for a shallow magma chamber beneath the Casa Diablo area does not preclude the existence of a magma chamber beneath the caldera. If present, the melt zone could have a very small spatial extent, or be located below or outside the area traversed by rays used in this study. The spatial resolution of the traveltime versus depth technique applied here depends on the availability of ray paths and the frequency band of the P or S waves transmitted through the magma body. The frequency response of the seismometers and the recording instruments makes it possible to study frequencies in the range 2 to 20 Hz, which corresponds to wavelengths of S waves of 0.15 to 1.5 km, assuming an S wave velocity of 3 km/s. If the melt zone can be modeled as a zone of very low $Q\beta$ (Sanders [1984] suggested $Q_\beta \sim 30$), the S waves may travel a few wavelengths before they can no longer be detected. Hence the spatial resolution of this technique may only be of the order of a few kilometers. In areas where no rays are available, as for instance, in the west moat of the caldera, a melt zone would not be detected by this experiment.

The intepretation of low S wave amplitudes as radiation pattern effects in this study suggests that other S wave shadowing studies such as those of Sanders [1984] should be reexamined. Sanders [1984] shows focal mechanisms from two earthquakes to illustrate that the S wave at one station is strongly attenuated. Although he shows both mechanisms as strike slip, it is clear that the second one could be a reverse mechanism since only 10 first-motion polarities are available. Hence the difference in focal mechanism may be sufficient to explain the one strongly attenuated S wave. The most fundamental drawback of Sanders' [1984] approach is the fact that he inspected seismograms from stations that only cover slightly more than one quadrant of the focal sphere, or approximately a 110° range in azimuth. One way of detecting radiation pattern effects would be to analyze seismograms for the full 360° range of azimuths. This could be accomplished by analyzing data from the U.S. Geological Survey seismic network located to the south and west.

Initially, Elbring and Rundle [1986] analyzed a subset of the seismograms included in this study. They used forward modeling based on two-dimensional ray tracing to infer two magma chambers beneath the caldera. The shallower chamber was located beneath Casa Diablo at a depth of 3.7 km and had dimensions of approximately 2 km by 3 km. The deeper, larger chamber was located at a depth of 5.5 km near the northern part of the resurgent dome. The results of this study, however, demonstrate that the reduced travel time depth profile for P waves used by Elbring and Rundle [1986], although a valid procedure, was incorrectly determined. The reduced travel time depth profile determined from this study shows no

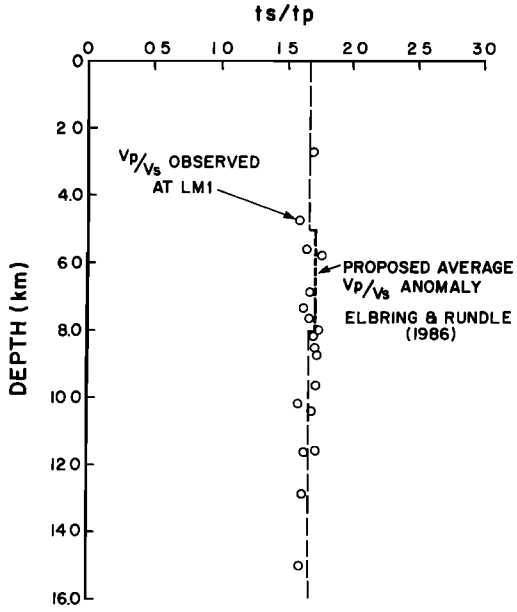

Fig. 12. Observed S travel time divided by observed P travel time at the borehole station (LM1) plotted as a function of hypocentral depth. The Vp/Vs ratio found by Elbring and Rundle [1986] is also plotted for comparison. Only data from the 19 events studied by Elbring and Rundle [1986] are included.

systematic variation of travel time with depth and hence does not support the shallow magma chambers proposed by Elbring and Rundle [1986].

In summary, more careful and extensive analysis of seismograms from local earthquakes in the Long Valley region is needed to establish if shallow magma chambers exist beneath the Long Valley caldera. Some of the studies carried out so far are inconclusive, since the investigators have not yet analyzed a sufficiently complete data set to properly address the question. Only one borehole has been available for deploying a downhole seismometer, but the results of this study serve to illustrate the usefulness of the high-quality data that can only be obtained from borehole instruments. A data set from a two-dimensional array of boreholes instrumented with downhole seismometers is needed to carry out a full-scale inversion for the velocity structure of the upper and middle crust beneath the Long Valley caldera.

Conclusions

The analysis of the high-quality borehole and surface seismograms consisted of (1) a search for S wave shadowing, (2) a search for travel time delays reported by Elbring and Rundle [1986], and (3) a search for travel time delays by comparing surface and downhole data.

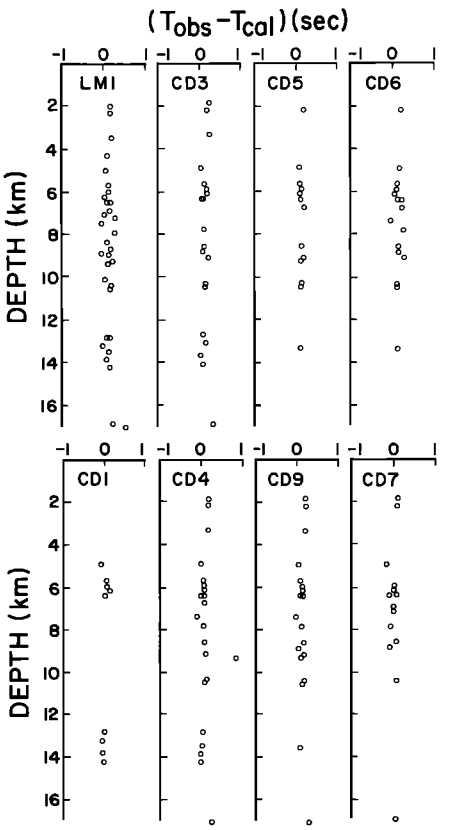

Fig. 13. Difference between observed and calculated travel time versus depth for the 32 earthquakes recorded both by the borehole (LM1) and surface stations (CD1-CD9). See also Figure 1. Note the absence of systematic travel time delays as a function of depth.

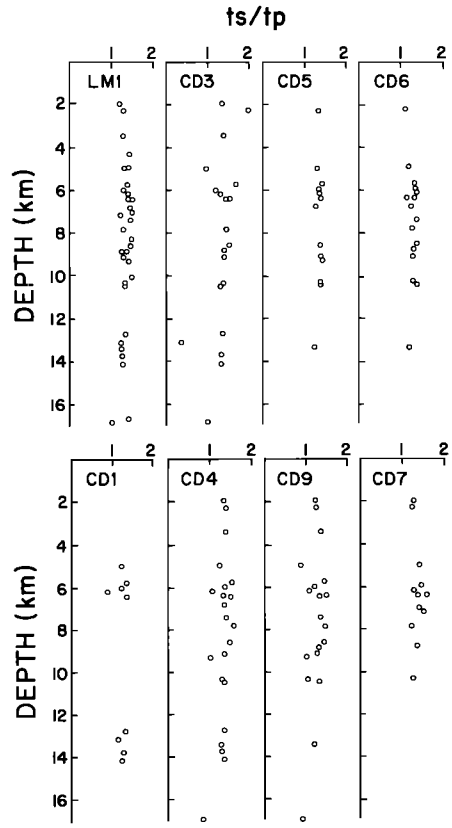

Fig. 14. Observed S travel time divided by observed P travel time plotted as a function of hypocentral depth for both the borehole (LM1) and surface stations (CD1-CD9). See also Figure 1. Note the absence of systematic variations in the Vp/Vs ratio as a function of depth.

Observed small S amplitudes relative to P amplitudes can be explained in terms of source radiation effects. The apparent travel time delays reported by Elbring and Rundle [1986] result from inaccurately calculated epicentral distances. A further comparison of the downhole and surface data shows no systematic travel time delays. In addition, the average Vp/Vs ratio as a function of depth remains fairly constant. These three independent methods of analysis provided no evidence for the presence of a magma chamber at shallow crustal levels beneath the Casa Diablo area in the Long Valley caldera. Hence the data from both downhole and surface stations suggest that a melt zone, if present beneath the caldera, has much smaller spatial dimensions than previously suggested or is located deeper (> 8-12 km depth) or outside the region traversed by the north-south traveling rays.

Acknowledgments. I thank L. M. Jones, T. L. Henyey, P. C. Leary, and N. E. Goldstein for reviews. T. McEvilly made ten DR-100 instruments available, and T. L. Teng made four DR-100 instruments available for this study. L. M. Jones, D. Manov, and J. Scott assisted with the field work. K. Ladd played back the original data cassettes to a more manageable computer format. K. Aki suggested normalizing

the P and S amplitudes with coda amplitudes. This research was supported by the Assistant Secretary for Renewable Energy, Office of Renewable Energy Technologies, Geothermal Technology Division of the U.S. Department of Energy under contract DE-AC03-76SF00098 to the Lawrence Berkeley Laboratory.

References

Aki, K., Scattering and attenuation, Bull. Seismol. Soc. Am., 72, S319-S330, 1982.

Aki, K., and P. G. Richards, Quantitative Seismology: Theory and Methods, W. H. Freeman, San Francisco, Calif., 1980.

Cockerham, R. S., and A. M. Pitt, Seismic activity in Long Valley caldera area, California: June 1982 through July 1984, U.S. Geol. Surv. Open File Rep., 84-939, 493-526, 1984.

Einarsson, P., S-wave shadows in the Krafla caldera in NE-Iceland, evidence for a magma chamber in the crust, Bull. Volcanol., 41(3), 1-9, 1978.

Elbring, G. J., and J. B. Rundle, Analysis of borehole seismograms from Long Valley, California: Implications for caldera structure, J. Geophys. Res., 91, 12,651-12,660, 1986.

Hill, D. P., Structure of Long Valley caldera from seismic refraction experiments, J. Geophys. Res., 81, 745-753, 1976.

Hill, D. P., E. Kissling, J. H. Luetgert, and U. Kradolfer, Constraints on the upper crustal structure of the Long Valley-Mono Crater Volcanic Complex eastern California, from seismic refraction measurements, J. Geophys. Res., 90, 11,135-11,150, 1985.

Kissling, E., W. L. Ellsworth, and R. S. Cockerham, Three-dimensional structure of the Long Valley Caldera, California, region by geotomography, U.S. Geol. Surv. Open File Rep., 84-939, 188-220, 1984.

Klein, F. W., User's guide to HYPOINVERSE, a program for VAX and PC350 computers to solve for earthquake locations, U.S. Geol. Surv. Open File Rep., 85-515, 1985.

Matumoto, T, Seismic body waves observed in the vicinity of Mt. Katmai, Alaska, and evidence for the existence of molten chambers, Bull. Geol. Soc. Am., 82, 2905-2920, 1971.

Reasenberg, P., and D. Oppenheimer, FPFIT, FPPLOT and FPPAGE: Fortran computer programs for calculating and displaying earthquake fault-plane solutions, U.S. Geol. Surv. Open File Rep., 85-739, 46 pp., 1985.

Rinehart, E. J., A. R. Sanford, and R. M. Ward, Geographic extent and shape of an extensive magma body at mid-crustal depths in the Rio Grande Rift near Socorro, New Mexico, in Rio Grande Rift: Tectonics and Magmatism, edited by R. E. Riecker, pp. 237-251, AGU, Washington, D. C., 1979.

Rundle, J. B., and J. Whitcomb, A model for deformation in Long Valley California, 1980-1983, J. Geophys. Res., 89, 9371-9380, 1984.

Ryall, A., and F. Ryall, Attenuation of P and S waves in a magma chamber in Long Valley caldera, California, Geophys. Res. Lett., 8, 557-560, 1981.

Sanders, C. O., Location and configuration of magma bodies beneath Long Valley, California, determined from anomalous earthquake signals. J. Geophys. Res., 89, 8287-8302, 1984.

Sanders, C. O., and F. Ryall, Geometry of magma bodies beneath Long Valley, California, determined from anomalous earthquake signals, Geophys. Res., Lett., 10(8), 690-692, 1983.

Savage, J. C., and M. M. Clarke, Magmatic resurgence in Long Valley Caldera, California: Possible cause of the 1980 Mammoth Lakes earthquakes, Science, 217, 531-533, 1982.

Savage, J. C., R. S. Cockerham, and J. E. Estrem, and L. R. Moore, Deformation near the Long Valley caldera, eastern California, J. Geophys. Res., 92, 2721-2746, 1987.

Steeples, D. W., and H. M. Iyer, Low-velocity zone under Long Valley as determined from teleseismic events, J. Geophys. Res., 81, 849-860, 1976.

E. Hauksson, Department of Geological Sciences, University of Southern California, Los Angeles, CA 90089-0740.

(Received June 3, 1987;
revised November 17, 1987;
accepted November 17, 1987.)